Journal of Magnetic Resonance 308 (2019) 106574

Contents lists available at ScienceDirect

Journal of Magnetic Resonance

journal homepage: www.elsevier.com/locate/jmr

TmDOTP: An NMR-based thermometer for magic angle spinning NMR experiments

Dongyu Zhang [a], Boris Itin [b], Ann E. McDermott [a,*]

[a] Department of Chemistry, Columbia University, New York, NY 10027, United States
[b] New York Structural Biology Center, New York, NY 10027, United States

ARTICLE INFO

Article history:
Received 12 March 2019
Revised 13 August 2019
Accepted 15 August 2019
Available online 16 August 2019

Keywords:
Nuclear magnetic resonance
Magic-angle spinning
Sample Heating
Real-time NMR temperature measurement
Dielectric loss
$TmDOTP^{5-}$

ABSTRACT

Solid state NMR is a powerful tool to probe membrane protein structure and dynamics in native lipid membranes. Sample heating during solid state NMR experiments can be caused by magic angle spinning and radio frequency irradiation such heating produces uncertainties in the sample temperature and temperature distribution, which can in turn lead to line broadening and sample deterioration. To measure sample temperatures in real time and to quantify thermal gradients and their dependence on radio frequency irradiation or spinning frequency, we use the chemical shift thermometer TmDOTP, a lanthanide complex. The H_6 TmDOTP proton NMR peak has a large chemical shift (−176.3 ppm at 275 K) and it is well resolved from the protein and lipid proton spectrum. Compared to other NMR thermometers (e.g., the proton NMR signal of water), the proton spectrum of TmDOTP, particularly the H_6 proton line, exhibits very high thermal sensitivity and resolution. In MAS studies of proteoliposomes we identify two populations of TmDOTP with differing temperatures and dependency on the radio frequency irradiation power. We interpret these populations as arising from the supernatant and the pellet, which is sedimented during sample spinning. In this study, we demonstrate that TmDOTP is an excellent internal standard for monitoring real-time temperatures of biopolymers without changing their properties or obscuring their spectra. Real time temperature calibration is expected to be important for the interpretation of dynamics and other properties of biopolymers.

1. Introduction

Magic angle spinning (MAS) solid-state nuclear magnetic resonance (SSNMR) is a powerful technique for studying biomolecules [1] including protein assemblies in near native conditions, [2] membrane proteins [3–5] and amyloid fibrils [6–8]. SSNMR provides atomic level information on protein molecular structure and motions. Restricted global molecular motions in solids allow for the retention of dipolar coupling, which enables direct measurement of distances and local orientations. Many of the most exciting developments in SSNMR, however, involve pulse sequences with long and strong radio frequency (RF) irradiation elements. Sample heating from magic angle spinning and RF irradiation has been a cause for concern [9,10]. Elevated and uncalibrated temperature within the sample complicates the interpretation of dynamics and other properties. Moreover, heating gradients within an MAS rotor may contribute to peak broadening.

Sample heating originates in part from friction between bearing gas and rotor during MAS [10,11]. Heat is also generated from RF irradiation during high power decoupling due to inductive and dielectric losses [9,12,13]. The inductive loss originates from dissipative eddy currents that are caused by oscillating B_1 field. The loss is proportional to the sample conductivity and increases quadratic with the frequency. Neither parameter is freely variable in practice for most experiments on biological samples [14]. Dielectric loss is derived from the dissipative interaction between electric dipoles or charges and the oscillating electric field originating from the potential difference across the coil. The absorption of RF energy is maximized when $\omega\tau = 1$, where ω represents the frequency of the oscillating field and τ is the characteristic relaxation time of the dipole [13,15]. The dielectric loss is not solely dependent on the sample conductivity and is thus difficult to calculate [16]. RF heating is of particular concern in SSNMR experiments on biological samples due to the resistive losses from the high concentration of ions in typical biological buffers and the dielectric losses from the presence of permanent dipoles such as constrained water molecules and hydrated lipids which have relaxation times on the order of the reciprocal B_1 frequency [9,15,17–19]. Therefore,

* Corresponding author.
E-mail address: aem5@columbia.edu (A.E. McDermott).

https://doi.org/10.1016/j.jmr.2019.106574
1090-7807/

attention has been placed on reducing dielectric losses by decreasing coil inductance, leading to advances such as scroll coil, z-coil, Doty XC coil and low-E coil, later adapted and commercialized by Bruker Biospin [20–23]. The low-E coil, used in this work, employs a crossed-coil design with a combination of a low-inductance loop gap resonator tuned to the proton frequency, and a solenoid coil tuned to lower frequencies [24]. Although this design reduces the heating relative to a standard solenoid, it is nevertheless of interest to characterize heating effects in a low-E probe in-situ and develop convenient tools to monitor the sample temperature in real time during SSNMR experiments.

Here, we use thulium 1,4,7,10-tetra-azacyclododecane-l,4,7,10-tetrakis (methylene phosphonate) $TmDOTP^{5-}$ (CAS: 30859-88-8), specifically the H_6 proton chemical shift in this compound, as an internal thermometer for biological samples during SSNMR experiments (Fig. 1A). $TmDOTP^{5-}$ is a water soluble paramagnetic complex, which is known to have strongly temperature dependent chemical shifts for ^{1}H, ^{13}C and ^{31}P (Fig. 1B) [25]. Compared with other compounds that have excellent thermal resolution in chemical shifts, such as $Pb(NO_3)_2$, KBr or $Sm_2Sn_2O_7$ [17], the proton spectrum of $TmDOTP^{5-}$ is convenient to measure as a solute in the sample of interest, i.e. without changing samples or probe tuning. The H_6 proton was chosen for its moderately high temperature sensitivity and relatively narrower linewidth as compared to the five other nonequivalent protons [26]. TmDOTP has previously been demonstrated to serve as a chemical shift thermometer in solution NMR and solid state NMR, and was used to characterize NMR probes in several studies [14,24,27]. Due to its low toxicity, $TmDOTP^{5-}$ has been applied to clinical magnetic resonance to measure the temperature of tissue cells and tumor cells during surgery [26].

2. Materials and methods

2.1. NMR sample preparation

TmDOTP (Macrocyclics, Inc.) solutions were made with 25 mM TmDOTP (molecular weight: 914.2 g/mol), 20 mM MOPS and 100 mM KCl at pH 7.5 in 99.96% D_2O (Sigma). Although this compound is very stable in biological media, the use of fresh material and verification with Mass Spec or NMR is advised because of finite shelf life of the compound. 10 mg wt-KcsA was overexpressed and reconstituted into 3:1 DOPE/DOPG (wt/wt) liposomes as described previously [28]. The proteoliposome sample was resuspended and incubated with a buffer containing TmDOTP (conditions as above) for 2 h before packing into a standard-wall zirconia Bruker 3.2 mm rotor with a silicon spacer on the top.

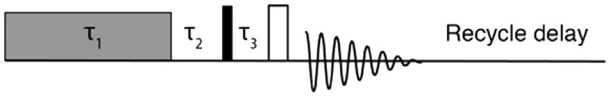

Fig. 2. ^{1}H pulse sequence used to measure the temperature increase from RF irradiation. The RF irradiation is applied for the duration of τ_1. τ_2 represents the delay before proton 90 pulse. A spin echo with $\tau_3 = 20$ μs is applied before acquisition to dephase the signal from H_1 in TmDOTP.

2.2. NMR spectroscopy

Experiments were carried out using a 3.2 mm standard-bore E-free probe and 1.3 mm HCN probe on a Bruker Avance II 900 MHz spectrometer. The temperature was regulated with VT gas (flow rate 1070 L/hr) and a heater in the probe. The temperature sensor is located in the probehead. The VT control unit was calibrated using the chemical shift difference between the —CH_3 and —OH groups of methanol [29]. The temperature of the system was allowed to equilibrate for at least 15 min after each temperature change. The pulse sequence used to measure heating from RF irradiation is shown in Fig. 2. τ_1 represents the duration of the heating pulse, which was selected to mimic typical times used for high power decoupling. Unless otherwise specified, τ_1 was 30 ms and the recycle delay was 1 s. τ_2 is a variable delay time to study cooling after irradiation. Owing to the short T_1 of the TmDOTP H_6 proton (~800 μs), τ_2 was typically 5 ms (unless otherwise specified), thus limiting heat dissipation before acquisition. A short spin echo ($\tau_3 = 40$ μs) is added before acquisition to suppress TmDOTP H_1 signals, which also has a larger temperature slope (ppm/K) and could interfere with H_6 signal at high temperature. The one-dimensional MAS spectra were acquired using 8 dummy scans and 512 co-added scans. The chemical shift of ^{1}H was externally referenced to DSS at 0 ppm.

The ^{13}C–^{13}C dipolar assisted rotational resonance (DARR [30]) experiments with 50 ms mixing time were performed on the same 900 MHz spectrometer with a MAS rate of 16.666 kHz and a set temperature of 267 K. Proton decoupling with the SPINAL64 [31] scheme at 90 kHz was applied during acquisition. The recycle delay was 2.5 s. The ^{1}H and ^{13}C Dual-Receiver DARR experiment was performed on 3.2 mm standard-bore E-free probe with Bruker Avance NEO spectrometer operating at 700 MHz. The MAS rate was 12.5 kHz and VT gas flow was 2000 L/h. SPINAL64 decoupling was applied at $\omega_1/2\pi = 90$ kHz on the proton channel during

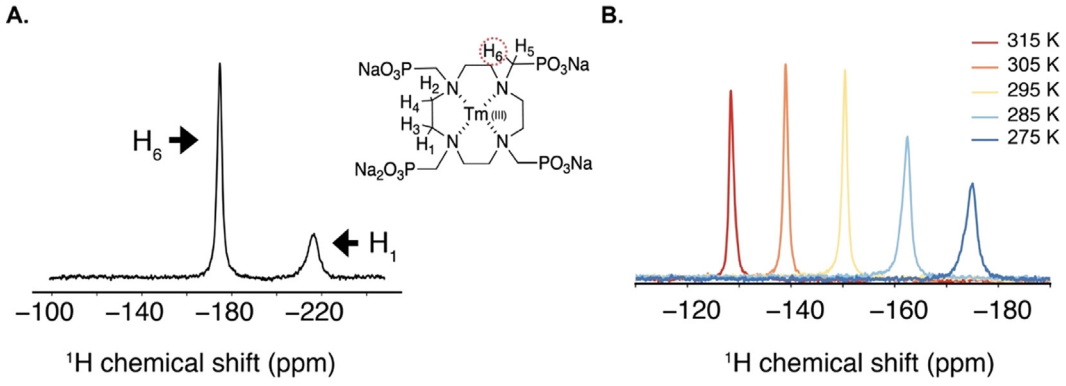

Fig. 1. (A) Molecular structure of TmDOTP with H_6 highlighted and portion of the ^{1}H NMR spectrum of 25 mM TmDOTP. The sample contains KcsA proteoliposome and 25 mM TmDOTP. H_6 is at −176.3 ppm while H_1 is −218.8 ppm. (B) Overlay of the spectra of the H_6 proton in TmDOTP acquired at various temperatures. All spectra were collected on 900 MHz with MAS frequency at 5 kHz. Chemical shift was referenced to the DSS at 0 ppm.

acquisition (15 ms) and the recycle delay was 2 s. All data were processed in NMRPipe and ^{13}C chemical shift was referenced to downfield line of Adamantane at 40.48 ppm relative to ^{13}C in DSS.

3. Results and discussion

3.1. ^{1}H NMR signals of H_2O and TmDOTP provide precise temperature measurements

The water chemical shift is known to be sensitive to temperature, and it has been employed as an internal thermometer in several studies [18,19,32]. We compared the temperature dependence of the chemical shift of the H_6 proton in TmDOTP to that of the water proton in the same sample on 900 MHz with 3.2 mm E-free probe (Fig. 3). The temperature dependence of the H_6 proton in TmDOTP, 1.06 ± 0.04 ppm/K, is 2 orders of magnitude larger than that of water (-1.1 × 10^{-2} ± 0.1 × 10^{-2} ppm/K), while the full width at half maximum (FWHM), (1.5 ± 0.6 ppm), is one order of magnitude larger than that of water (0.12 ± 0.01 ppm). The uncertainty in the calculated temperature dependencies were dominated by fitting error from linear least square fitting. The errors from chemical shift reading and temperature calibration are both a magnitude smaller than the fitting error. Overall, TmDOTP allows for more accurate and precise temperature measurements than water. The homogeneous linewidth of the H_6 proton calculated from $1/\pi T_2$ was about 980 ± 60 Hz at the sample temperature of 276.5 ± 0.1 K (with a VT gas temperature of 275 K and spinning frequency at 5 kHz). The offset between homogeneous linewidth and the actual linewidth, 2.2 kHz (acquired at the same temperature) is presumably due to inhomogeneous broadening.

3.2. Sample heating due to spinning is proportional to the rotor frequency squared

MAS induced sample heating was measured in a 3.2 mm E-free probe (Fig. 4) and a 1.3 mm probe (Fig. S2). Samples containing just

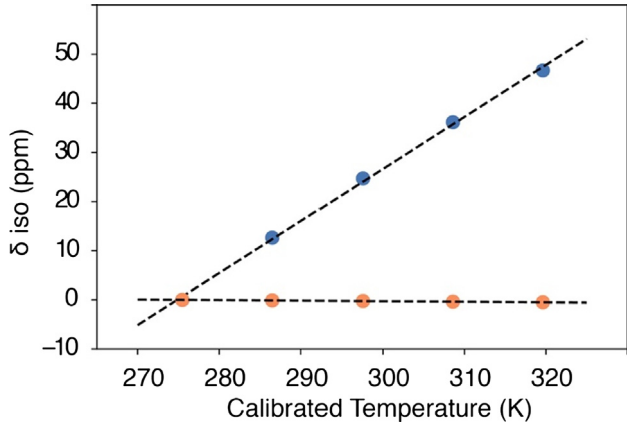

Fig. 3. The temperature dependence of the chemical shift of the H_6 proton in TmDOTP (blue) and of the water proton (orange). $\Delta\delta_{iso}$ is the change in chemical shift relative to the shift at VT gas temperature of 275 K. All spectra were collected on a Bruker Avance II 900 MHz spectrometer equipped with a 3.2 mm standard-bore E-free probe. The spinning frequency was 5 kHz and the gas flow rate was 1070 L/h. The dashed lines represent a linear least squares optimized fit to the data: $\delta iso_{,TmDOTP} = 1.06(\frac{ppm}{K})T - 291$ (ppm); $\delta iso_{,water} = -0.011(\frac{ppm}{K})T + 3.03(ppm)$. The uncertainties are the stand error of regression slope, ±0.04 ppm/K and ±0.1 × 10^{-2} ppm/K for TmDTOP and water respectively. The error bars in both x and y dimensions for each data point are on the magnitude of 1 × 10^{-3}. The ratio of slope and FWHM for TmDOTP and water are 0.7 ± 0.3 and 0.09 ± 0.01 respectively. The expansion of water chemical shift vs. calibrated temperature is shown in supplementary information (Fig. S1). (For interpretation of the references to color in this figure legend, the reader is referred to the web version of this article.)

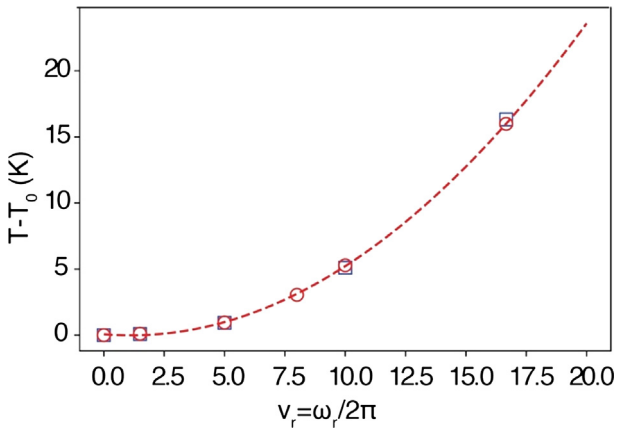

Fig. 4. Sample temperature calculated from the chemical shift of the H_6 proton of TmDOTP as a function of spinning frequency. T_0 is the temperature at zero spinning asymptote. TmDOTP buffer (red open circle) and KcsA proteoliposome samples (blue open square) were characterized to demonstrate that the MAS induced heating is similar for aqueous samples. Data for the TmDOTP buffer were fit to a second order polynomial function (red dash line): $T = 67\frac{mK}{Hz^2}\upsilon_r^2 - 148\frac{mK}{Hz}\upsilon_r + 65mKT$. Data for the 1.3 mm probe is shown in the supplementary information (Fig. S2). (For interpretation of the references to color in this figure legend, the reader is referred to the web version of this article.)

TmDOTP buffer and those containing KcsA proteoliposomes were used to demonstrate that the MAS heating is sample independent. The spinning frequencies and the corresponding sample temperatures of TmDOTP were fit to a second-order polynomial function analogously to previous studies: $T = 67\frac{mK}{Hz^2}\upsilon_r^2 - 148\frac{mK}{Hz}\upsilon_r + 65mK$, where $\upsilon_r = \frac{\omega_r}{2\pi}$. Notably, the H_6 proton linewidth increased consistently with spinning frequency from 1636 Hz (at 2 kHz MAS) to 3663 Hz (at 16 kHz MAS). This increase in linewidth with increasing MAS frequency suggests that a gradient in temperature across the sample was caused by MAS. The line shape also became increasingly asymmetric with increasing MAS.

3.3. The influence of TmDOTP on hydrated proteoliposome samples

We compared the KcsA proeoliposome spectra with and without including 25 mM TmDOTP in the preparation. We observed no significant changes in chemical shifts or overall spectral quality (Fig. 5A). KcsA, a pH activated potassium channel from *Streoptomyces lividans*, is used here since the marker peaks of the protein are known to be sensitive to pH, temperature and potassium ion concentration changes [3,28]. This result suggests that the paramagnetic nature of the TmDOTP complex has little to no effect on the properties of biological samples at the concentrations used. Marker peaks that have been assigned to the water exposed selectivity filter residues T74, T75 and V76 are specifically examined here (Fig. 5B–D).

3.4. RF heating is linear with pulse power, pulse length and duty cycle

To examine the heating of a biological sample during RF irradiation, the pulse sequence shown in Fig. 2 was applied to a KcsA proteoliposome sample and the temperature was monitored using the chemical shift of the H_6 proton in TmDOTP. The VT gas temperature was 275 K and the cooling gas flow rate was 1070 L/hr. Continuous wave (CW) irradiation (following typical proton heteronuclear decoupling field strengths) was applied and the RF power, pulse duration (τ_1), and duty cycle were varied. τ_2 was kept small (5 ms) to limit sample cooling before acquisition. Fig. 6 shows that heating is proportional to the RF power, duration of

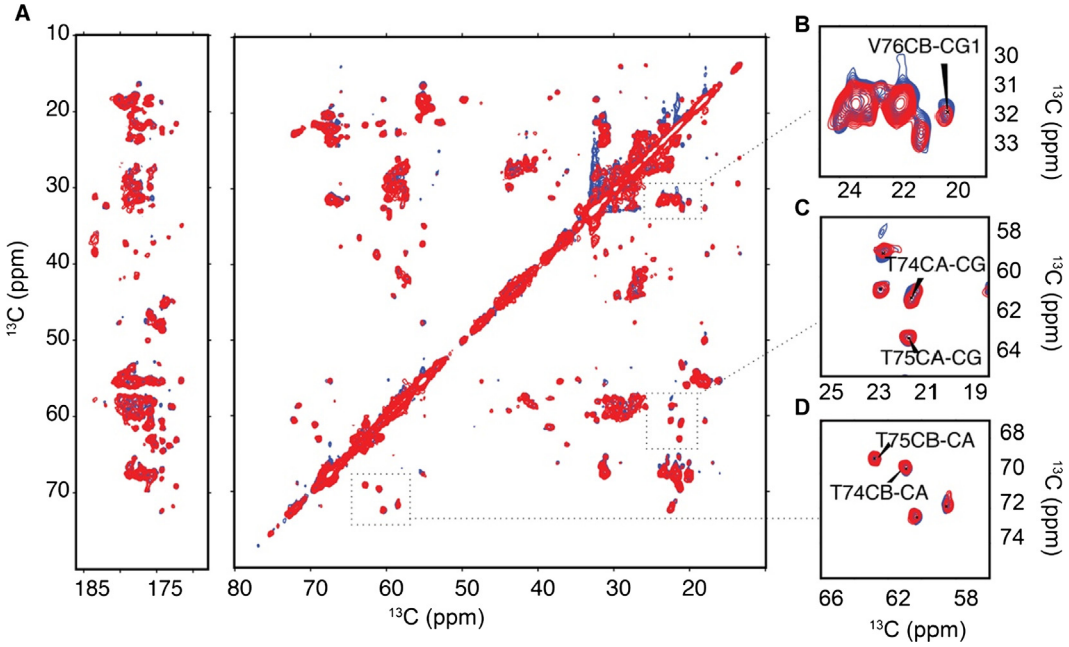

Fig. 5. KcsA proteoliposome spectra with and without 25 mM TmDOTP. (A) Overlay of 2D ^{13}C–^{13}C correlation spectra of KcsA (blue) and KcsA with 25 mM TmDOTP (red) both in DOPE/DOPG (3:1) liposomes at pH7.5. Spectral regions containing KcsA selectivity filter marker peaks are highlighted and shown in (B) V76 Cβ-Cγ (C) T74 Cα-Cγ and T75 Cα-Cγ (D) T74 Cβ-Cα and T75 Cβ-Cα. The data suggest no significant changes in protein structure and conformation state, and no changes in spectral quality with the addition of 25 mM TmDOTP. (For interpretation of the references to color in this figure legend, the reader is referred to the web version of this article.)

the pulse and duty cycle as expected and documented in prior literatures [13,18].

3.5. Inequivalent RF heating on pellet vs. supernatant

One surprising finding from our RF irradiation study on the proteoliposome KcsA sample is that the H_6 proton in TmDOTP peak splits into two components (denoted by peak 1 and peak 2) under RF irradiation on 3.2 mm E-free probe (Fig. 7). Peak 2, with a larger heating slope, only appeared under RF heating conditions, but not with MAS heating alone (Fig. S3). Moreover, the temperature reported by peak 2 matches the one calculated from the water proton chemical shift in the sample (Fig. S4). However, the two distinct temperature populations are not well resolved for the water proton peaks due to the broad linewidth (130 Hz) and gradient in temperatures. We assigned the two peaks to TmDOTP in a pellet (peak 1) that sediments to the inner rotor wall due to the centrifugal forces generated by MAS and to the TmDOTP remaining in the supernatant (peak 2) based in prior work [33,34]; this assignment resulted in good agreement of the temperature determined using the TmDOTP frequency with the temperature based on the water peak positions. The homogeneous linewidth calculated from T_2 for peaks 1 and 2 are 815 ± 39 Hz and 598 ± 22 Hz respectively. The divergent temperatures for the pellet vs. supernatant might arise from different cooling speeds along the radial axis of the rotor and the distinct heat capacity of water vs. proteoliposome.

Data collected using a 1.3 mm solenoid probe is shown in Fig. S5. At the same field strength, the distribution of temperatures

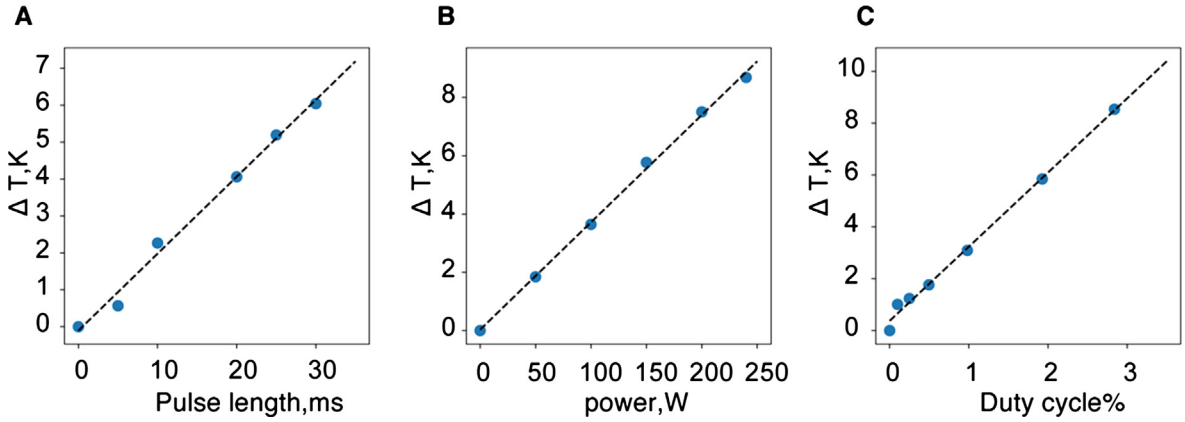

Fig. 6. (A) The temperature increase indicated by the TmDOTP chemical shift is linearly dependent on the RF pulse length (field strength = 91 kHz, duty cycle = 2.8%). Data were fit using a linear least square analysis ($\Delta T = 0.208\tau_1 - 0.105$). (B) The dependence on CW power amplitude is shown ($\tau_1 = 30$ *ms and duty cycle* = 2.8%). Data were fit using linear least square function ($\Delta T = 0.037P + 0.032$), P represents RF power. (C) The dependence on duty cycle percentage is shown (field strength = 91 kHz and $\tau_1 = 30$ *ms*, $\tau_2 = 5$ *ms*); in these experiments the duty cycle is varied by varying the recycle delay from 0.5 s to 15 s. Data were fit using linear least square analysis ($\Delta T = 2.860D + 0.375$). D represents the duty cycle percentage. All data were collected on a KcsA proteoliposome sample with 20 mM TmDOTP and a 3.2 mm E-free probe on 900 MHz. The spinning frequency was 5 kHz with sample temperature of 276.5 ± 0.1 K (VT gas temperature was 275 K).

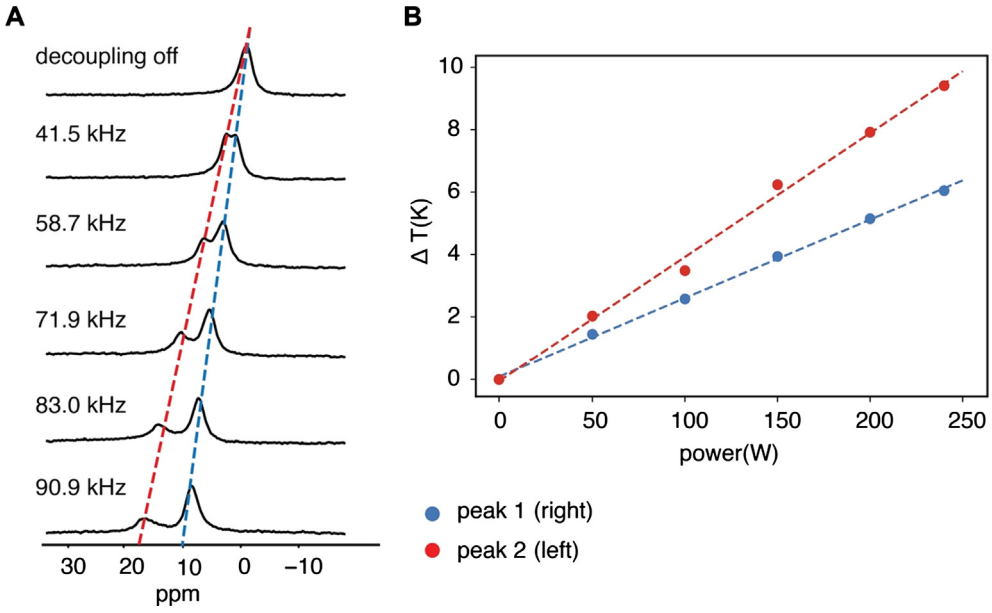

Fig. 7. (A) The H_6 NMR spectra of the proteoliposome sample with 20 mM TmDOTP at neutral pH during different RF frequencies. The VT gas temperature was 275 K. The chemical shift of H_6 is reported relative to that with the decoupling pulse off. Conveniently, TmDOTP has a slope of 1.06 ± 0.04 ppm/K. (B) The sample temperature changes reported by the peak 1 and peak 2 from TmDOTP proton chemical shifts are plotted as a function of the RF power. Data were collected on the 3.2 mm E-free probe at 900 MHz.

observed in the sample is consistently higher on the 1.3 mm solenoid probe as compared with a 3.2 mm E-free probe. The 1.3 mm solenoid exhibited a considerable and continuous heating gradient, which was estimated from the linewidth as 18 K at a field strength of 90 kHz. A significantly reduced RF loss and reduced heating and temperature gradient was observed on 3.2 mm E-free probe due to the mitigation of dielectric loss by a low-inductance loop gap resonator coil.

3.6. Application and significance

Owing to its minimal perturbation of biological sample properties, TmDOTP can be incorporated into SSNMR samples to monitor real time temperature throughout an experiment. This may be crucial for measurements that are sensitive to temperature changes, such as relaxation experiments [35]. Here, we demonstrate the temperature mapping of a ^{13}C–^{13}C dipolar assisted rotational resonance (DARR) experiment using 20 mM TmDOTP in KcsA proteoliposome sample. The experiment was carried out at Bruker 700 MHz equipped with a 3.2 mm E-Free probe under 12.5 kHz MAS. The multi-receiver feature on AVANCE NEO enabled a H_6 chemical shift measurement promptly following each carbon acquisition. Fig. S6 shows that the temperature of the KcsA sample increased about 0.5 K during the experiment due to high power (90 kHz) proton decoupling during the increasing evolution time (t1). In addition, our data demonstrate that heating from MAS and RF radiation are not additive. In order to obtain the precise temperature during an experiment, it is useful to include a real time thermometer, such as TmDOTP, rather than a simple extrapolation (Fig. S7).

4. Conclusion

With a linear temperature dependency and large thermal resolution, TmDOTP is an excellent internal thermometer for solid state NMR experiments on biological samples. The distinct proton chemical shift and short T_1 enable real time in situ indication of the precise temperature in a biological sample. Compared with common thermometer molecules employed in SSNMR, such as ^{207}Pb in $Pb(NO_3)_2$, ^{119}Sn in $Sm_2Sn_2O_7$, and KBr, TmDOTP stands out in its low toxicity and nearly negligible perturbations on sample properties. Moreover, the proton detection can be performed without a change in the probe configuration, enabling real time temperature readings during an experiment. We observed two temperature populations in KcsA proteoliposome samples induced by RF irradiation. The two peaks were assigned to the pellet at the inner rotor wall and the central supernatant that result from MAS centrifugation.

Acknowledgments

The NMR data was collected at the New York Structural Biology Center (NYSBC) with the support from the Center on Macromolecular Dynamics by NMR Spectroscopy (CoMD/NMR) a Biomedical Technology Research Resource (BTRR) supported by U.S. National Institutes of Health (NIH) through grant number: P41 GM118302. The NYSBC is also supported by a grant from the Empire State Division of Science Technology and Innovation and Office of Research Infrastructure Programs/NIH Facility Improvement Grant CO6RR015495. A.E.M. is a member of the NYSBC. This work was supported by NIH Grant R01 GM088724 (to A.E.M). Authors thank Dr. Jochem Struppe (Bruker Biospin) for help with Dual Detection experiment set up.

Appendix A. Supplementary material

Supplementary data to this article can be found online at https://doi.org/10.1016/j.jmr.2019.106574.

References

[1] A. McDermott, Structure and dynamics of membrane proteins by magic angle spinning solid-state NMR, Annu. Rev. Biophys. 38 (2009) 385–403, https://doi.org/10.1146/annurev.biophys.050708.133719.
[2] S. Gupta, R. Tycko, Segmental isotopic labeling of HIV-1 capsid protein assemblies for solid state NMR, J. Biomol. NMR. 70 (2018) 103–114, https://doi.org/10.1007/s10858-017-0162-1.
[3] B.J. Wylie, M.P. Bhate, A.E. McDermott, Transmembrane allosteric coupling of the gates in a potassium channel, Proc. Natl. Acad. Sci. 111 (2014) 185–190, https://doi.org/10.1073/pnas.1319577110.

[4] Y. Zhao, H. Xie, L. Wang, Y. Shen, W. Chen, B. Song, Z. Zhang, A. Zheng, Q. Lin, R. Fu, J. Wang, J. Yang, Gating mechanism of aquaporin Z in synthetic bilayers and native membranes revealed by solid-state NMR spectroscopy, J. Am. Chem. Soc. 140 (2018) 7885–7895, https://doi.org/10.1021/jacs.8b03446.
[5] S.Y. Liao, K.J. Fritzsching, M. Hong, Conformational analysis of the full-length M2 protein of the influenza A virus using solid-state, NMR 22 (2013) 1623–1638, https://doi.org/10.1002/pro.2368.
[6] A.M. Barclay, D.D. Dhavale, J.M. Courtney, P.T. Kotzbauer, C.M. Rienstra, Resonance assignments of an α-synuclein fibril prepared in Tris buffer at moderate ionic strength, Biomol. NMR Assign. 12 (2018) 195–199, https://doi.org/10.1007/s12104-018-9808-5.
[7] C.P. Jaroniec, C.E. MacPhee, V.S. Bajaj, M.T. McMahon, C.M. Dobson, R.G. Griffin, High-resolution molecular structure of a peptide in an amyloid fibril determined by magic angle spinning NMR spectroscopy, Proc. Natl. Acad. Sci. 101 (2004) 711–716, https://doi.org/10.1073/pnas.0304849101.
[8] M. Mompeán, W. Li, J. Li, S. Laage, A.B. Siemer, G. Bozkurt, H. Wu, A.E. McDermott, The structure of the necrosome RIPK1-RIPK3 core, a human hetero-amyloid signaling complex, Cell 173 (2018) 1244–1253.e10, https://doi.org/10.1016/j.cell.2018.03.032.
[9] J.B. D'Espinose De Lacaillerie, B. Jarry, O. Pascui, D. Reichert, "cooking the sample": radiofrequency induced heating during solid-state NMR experiments, Solid State Nucl. Magn. Reson. 28 (2005) 225–232, https://doi.org/10.1016/j.ssnmr.2005.09.005.
[10] J. Brus, Heating of samples induced by fast magic-angle spinning, Solid State Nucl. Magn. Reson. 16 (2000) 151–160, https://doi.org/10.1016/S0926-2040(00)00061-8.
[11] A.R. Grimmer, A. Kretschmer, V.B. Cajipe, Influence of magic angle spinning on sample temperature, Magn. Reson. Chem. 35 (1997) 86–90, https://doi.org/10.1002/(SICI)1097-458X(199702)35:2<86::AID-OMR34>3.0.CO;2-2.
[12] D.S. McNair, Heat transfer in NMR of conductive samples with radiofrequency decoupling, J. Magn. Reson. 45 (1981) 490–502, https://doi.org/10.1016/0022-2364(81)90155-4.
[13] J.J. Led, S.B. Petersen, Heating effects in carbon-13 NMR spectroscopy on aqueous solutions caused by proton noise decoupling at high frequencies, J. Magn. Reson. 32 (1978) 1–17, https://doi.org/10.1016/0022-2364(78)90069-0.
[14] P.L. Gor'kov, W.W. Brey, J.R. Long, Probe development for biosolids NMR spectroscopy, in: Encycl. Magn. Reson., John Wiley & Sons, Ltd, Chichester, UK, 2010, pp. 1–13. doi: 10.1002/9780470034590.emrstm1149.
[15] C. Li, Y. Mo, J. Hu, E. Chekmenev, C. Tian, F.P. Gao, R. Fu, P. Gor'kov, W. Brey, T.A. Cross, F. Philip, R. Fu, P. Gor, W. Brey, T.A. Cross, Analysis of RF heating and sample stability in aligned static solid-state NMR spectroscopy, J. Magn. Reson 180 (2006) 51–57, https://doi.org/10.1016/j.jmr.2006.01.013.
[16] D.G. Gadian, F.N.H. Robinson, Radiofrequency losses in NMR experiments on electrically conducting samples, J. Magn. Reson. 34 (1979) 449–455, https://doi.org/10.1016/0022-2364(79)90023-4.
[17] D.J. Fowler, M.J. Harris, L.K. Thompson, Heat management strategies for solid-state NMR of functional proteins, J. Magn. Reson. 222 (2012) 112–118, https://doi.org/10.1016/j.jmr.2012.06.010.
[18] S.V. Dvinskikh, V. Castro, D. Sandström, Heating caused by radiofrequency irradiation and sample rotation in 13C magic angle spinning NMR studies of lipid membranes, Magn. Reson. Chem. 42 (2004) 875–881, https://doi.org/10.1002/mrc.1477.
[19] J. Wang, Z. Zhang, W. Zhao, L. Wang, J. Yang, Heating and temperature gradients of lipid bilayer samples induced by RF irradiation in MAS solid-state NMR experiments, Magn. Reson. Chem. 54 (2016) 753–759, https://doi.org/10.1002/mrc.4450.
[20] B. Dillmann, K. Elbayed, H. Zeiger, M.C. Weingertner, M. Piotto, F. Engelke, A novel low-E field coil to minimize heating of biological samples in solid-state multinuclear NMR experiments, J. Magn. Reson. 187 (2007) 10–18, https://doi.org/10.1016/j.jmr.2007.02.018.
[21] S.C. Grant, L.A. Murphy, R.L. Magin, G. Friedman, Analysis of multilayer radio frequency microcoils for nuclear magnetic resonance spectroscopy, IEEE Trans. Magn. 37 (2001) 2989–2998, https://doi.org/10.1109/20.947051.
[22] F.D. Doty, J. Kulkarni, C. Turner, G. Entzminger, A. Bielecki, Using a cross-coil to reduce RF heating by an order of magnitude in triple-resonance multinuclear MAS at high fields, J. Magn. Reson. 182 (2006) 239–253, https://doi.org/10.1016/j.jmr.2006.06.031.
[23] P.L. Gor'kov, E.Y. Chekmenev, C. Li, M. Cotten, J.J. Buffy, N.J. Traaseth, G. Veglia, W.W. Brey, Using low-E resonators to reduce RF heating in biological samples for static solid-state NMR up to 900 MHz, J. Magn. Reson. 185 (2007) 77–93, https://doi.org/10.1016/j.jmr.2006.11.008.
[24] S.A. McNeill, P.L. Gor'kov, J. Struppe, W.W. Brey, J.R. Long, Optimizing ssNMR experiments for dilute proteins in heterogeneous mixtures at high magnetic fields, Magn. Reson. Chem. 45 (2007) S209–S220, https://doi.org/10.1002/mrc.2146.
[25] C.S. Zuo, K.R. Metz, Y. Sun, A.D. Sherry, NMR temperature measurements using a paramagnetic lanthanide complex, J. Magn. Reson. 133 (1998) 53–60, https://doi.org/10.1006/jmre.1998.1429.
[26] C.S. Zuo, J.L. Bowers, K.R. Metz, T. Nosaka, A.D. Sherry, M.E. Clouse, TmDOTP5-: a substance for NMR temperature measurements in vivo, Magn. Reson. Med. 36 (1996) 955–959, https://doi.org/10.1002/mrm.1910360619.
[27] J.A. Stringer, C.E. Bronnimann, C.G. Mullen, D.H. Zhou, S.A. Stellfox, Y. Li, E.H. Williams, C.M. Rienstra, Reduction of RF-induced sample heating with a scroll coil resonator structure for solid-state NMR probes, J. Magn. Reson. 173 (2005) 40–48, https://doi.org/10.1016/j.jmr.2004.11.015.
[28] Y. Xu, M.P. Bhate, A.E. McDermott, Transmembrane allosteric energetics characterization for strong coupling between proton and potassium ion binding in the KcsA channel, Proc. Natl. Acad. Sci. 201701330 (2017), https://doi.org/10.1073/pnas.1701330114.
[29] C. Ammann, P. Meier, A. Merbach, A simple multinuclear NMR thermometer, J. Magn. Reson. 46 (1982) 319–321, https://doi.org/10.1016/0022-2364(82)90147-0.
[30] K. Takegoshi, S. Nakamura, T. Terao, 13C–1H dipolar-assisted rotational resonance in magic-angle spinning NMR, Chem. Phys. Lett. 344 (2001) 631–637, https://doi.org/10.1016/S0009-2614(01)00791-6.
[31] B.M. Fung, A.K. Khitrin, K. Ermolaev, An improved broadband decoupling sequence for liquid crystals and solids 101 (2000) 97–101.
[32] R. Linser, V. Chevelkov, A. Diehl, B. Reif, Sensitivity enhancement using paramagnetic relaxation in MAS solid-state NMR of perdeuterated proteins, J. Magn. Reson. 189 (2007) 209–216, https://doi.org/10.1016/j.jmr.2007.09.007.
[33] I.V. Sergeyev, S. Bahri, L.A. Day, A.E. McDermott, Pf1 bacteriophage hydration by magic angle spinning solid-state NMR, J. Chem. Phys. 141 (2014) 22D533, https://doi.org/10.1063/1.4903230.
[34] A. Böckmann, C. Gardiennet, R. Verel, A. Hunkeler, A. Loquet, G. Pintacuda, L. Emsley, B.H. Meier, A. Lesage, Characterization of different water pools in solid-state NMR protein samples, J. Biomol. NMR. 45 (2009) 319–327, https://doi.org/10.1007/s10858-009-9374-3.
[35] C.M. Quinn, A.E. Mcdermott, Quantifying conformational dynamics using solid-state R 1ρ experiments, J Magn Reson. 222 (2012) 1–7, https://doi.org/10.1016/j.jmr.2012.05.014.